Surface hardening and self-organized fractality through etching of random solids

A. Gabrielli,[1] A. Baldassarri,[1,2] and B. Sapoval[1,2]
[1]*Laboratoire de la Physique de la Matiere Condensée, Ecole Polytechnique - CNRS, 91128 Palaiseau, France*
[2]*Centre de Mathématiques et de leurs Applications, Ecole Normale Supérieure - CNRS, 94140 Cachan, France*
(Received 18 February 2000)

When a finite volume of etching solution is in contact with a disordered solid, complex dynamics of the solid-solution interface develop. If the etchant is consumed in the chemical reaction, the dynamics stop spontaneously on a self-similar fractal surface. As only the weakest sites are corroded, the solid surface gets progressively harder and harder. At the same time, it becomes rougher and rougher uncovering the critical spatial correlations typical of percolation. From this, the chemical process reveals the latent percolation criticality hidden in any random system. Recently, a simple minimal model was introduced by Sapoval *et al.* to describe this phenomenon. Through analytic and numerical study, we obtain a detailed description of the process. The time evolution of the solution corroding power and of the distribution of resistance of surface sites is studied in detail. This study explains the progressive hardening of the solid surface. Finally, this dynamical model appears to belong to the universality class of gradient percolation.

PACS number(s): 64.60.Ak, 81.65.Cf, 68.35.Bs

I. INTRODUCTION

Corrosion of solids has major economical consequences [1,2]. It is also interesting from the point of view of theoretical physics of random systems [3–7].

The comprehension of the basic physical mechanisms involved in corrosion implies the study of the dynamical evolution of the corrosion process and that of the morphological features of the corroded surface.

This paper presents a detailed study of a minimal model inspired by recent experiments on pit corrosion of aluminum thin films by an appropriate etching solution [8]. This two-dimensional model is a simplified etching model. It was first introduced in [9], where a preliminary numerical study has been developed. It provides a simple description for the action of a finite volume of a corroding solution on the surface of a disordered solid.

When an etching solution is in contact with an initially flat surface of a disordered solid, it starts to corrode its weakest regions and the surface gets ''harder.'' However, at the same time, new regions are discovered which contain weak elements. Depending on the corrosion reaction mechanism, different situations for this hardening process can occur.

Often the corrosive power of the solution is proportional to an etchant concentration. If the etchant is consumed in the reaction, then the corrosive power of a *finite volume* of solution decreases during the time evolution of the process. As the solid surface gets ''harder and harder,'' and the corroding power of the solution gets ''weaker and weaker,'' the corrosion process stops spontaneously in a finite time interval. At this moment all the surface sites are ''too hard'' to be etched by the solution.

It is this phenomenon which is studied both numerically and analytically in this paper.

A most interesting aspect of this kind of dynamical corrosion is that the final surface has a fractal geometry, showing that the corrosion mechanism itself uncovers the spatial correlations among the strong sites belonging to the solid. This is why this phenomenon is intimately related to percolation properties of random systems. In that sense this kind of corrosion reveals a ''latent'' criticality embedded in any random system.

The model reproduces qualitatively the same phenomenology observed experimentally [8]. The dynamical evolution can be divided into two different regimes.

(i) In the first (smooth) regime, the corrosion is well directed and the front becomes progressively rougher and rougher. In our model this regime does not depend on the details of the discretization chosen, nor even on the fundamental geometrical features of the lattice, such as the embedding space dimension or the lattice coordination number.

(ii) In the second regime, the correlations revealed by the hardening process become important: the dynamics becomes locally isotropic generating a fractal front. This corresponds to a critical regime, directly related to the static percolation transition on the same lattice.

The hardness of the final interface, which is related to the final corrosion power of the solution, depends on the external parameters such as the volume of the solution itself and the system size. When the volume of the solution is not too large, one observes a geometrical scaling regime. This regime corresponds to the scaling regime of a static percolation model known as ''gradient percolation.'' When the volume is increased, the correlation length grows to reach the system size. Above this limit, the finite-size effects dominate the behavior, and we do not study this case here.

II. MODEL

We first recall the two-dimensional etching model introduced in [9]. Its schematic is shown in Fig. 1.

(i) The solid is represented as a site lattice (triangular or square), of linear width L and, eventually, infinite depth.

(ii) A random number $r_i \in [0,1]$ (extracted from the flat probability density function $\pi_0(r)=1$ for $r \in [0,1]$) is assigned to each solid site i, representing its resistance to the etching by the solution. r_i does not depend on time (quenched disorder) nor on the site environment.

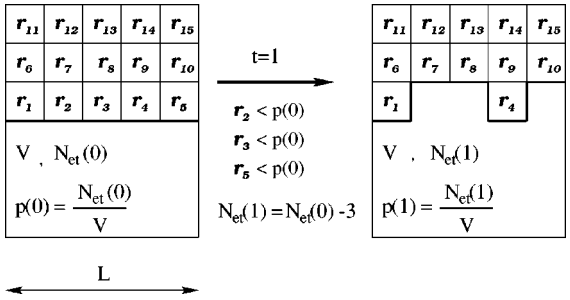

FIG. 1. Sketch of the etching dynamics in a square lattice: the sites 2,3,5 are etched at the first time step as their resistances are lower than $p(0)$. Consequently, the number of etchant particles in the solution decreases by three units. At $t=1$, the new interface sites are 7,8,10 if the solution can etch only the first-nearest-neighbor solid sites, or the whole second layer if the solution can also etch the second nearest neighbors in a diagonal direction.

(iii) The etching solution has a volume V and is initially in contact with the solid through the bottom boundary (see Fig. 1). It contains an initial number $N_{et}(0)$ of dissolved etchant molecules.

Consequently, the initial concentration $C(0)$ of etchant in the solution is given by $C(0)=N_{et}(0)/V$. Calling $N_{et}(t)$ the number of etchant molecules at time t, $C(t)=N_{et}(t)/V$. At each time step, the ''etching power'' of the solution (i.e., the average ''force'' exerted by the solution on a solid surface particle) is supposed to be proportional to $C(t)$: $p(t)=\Gamma C(t)$. Hereafter the assumption $\Gamma=1$ is made, without loss of generality. It implies $C(t)\equiv p(t)$. At time step t, all the interface sites with $r_i<p(t)$ are dissolved and a particle of etchant is consumed for each of these corroded solid sites.

Let us call $n(t)$ the number of dissolved solid sites at time t. One can express many important dynamical quantities through $n(t)$, or its time integral $N(t)$, that is, the total number of corroded solid sites up to time t. The number of etchant particles in the liquid will decrease as

$$N_{et}(t+1)=N_{et}(t)-n(t)=N_{et}(0)-N(t), \tag{1}$$

and consequently the etching power of the solution is

$$p(t+1)=p(t)-\frac{n(t)}{V}=p(0)-\frac{N(t)}{V}. \tag{2}$$

Note that, as $p(t+1)<p(t)$, a site having resisted to etching at a certain time step will resist forever. Consequently, the part of the solid surface which can be etched at time step $t+1$ is restricted to the sites which have just been uncovered by the etching process at time t. We call this subset of surface the ''active'' part of the surface. After a given time step, all the solid sites which have been previously explored by the solution are definitely ''passive.'' However, it may happen that ''passive'' sites are disconnected from the bulk at a later time step if they are connected to the solid by weak sites.

A. Phenomenological description of the dynamics

A typical process at two intermediate times, and at the final time step, is shown in Fig. 2.

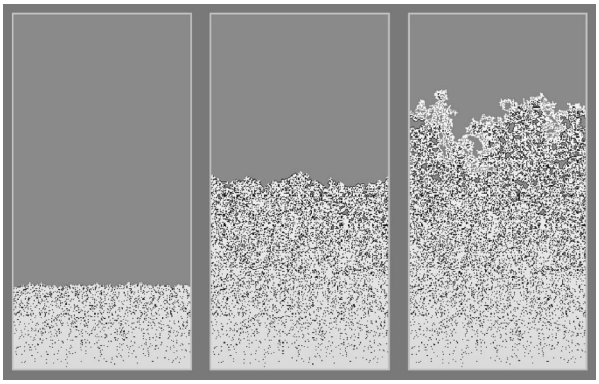

FIG. 2. Typical process represented at two intermediate time steps and at the final one. The solid is represented in gray, the solution in white, and the finite-size solid clusters detached by the solution in black. The final solid surface is found to be fractal up to a characteristic scale σ.

Some finite solid clusters are detached from the ''infinite'' solid by the corrosion process. Consequently, at any time, the ''global surface'' of the system is composed by both the finite clusters surfaces and the surface of the infinite solid, which will be called the ''corrosion front.'' Note that, in order to have a meaningful geometrical and physical definition of the solution space and of the connected solid regions (and then of the corrosion front), one has to use the so-called ''dual'' connection rules for solution and solid, respectively [10]. For example, on the square lattice, if the solution etches both first and second nearest neighbors, only first-nearest-neighbor solid sites should be considered as connected. On the other side, if the solution etches only the first nearest neighbor, both first- and second-nearest-neighbor solid sites should be considered as connected. On the triangular lattice, if the solution etches first nearest neighbors, liquid and solid sites are considered to be connected both by first nearest neighbors only.

Two remarks should be made.

(i) The corrosion front stays quite smooth at the beginning of the dynamics (first snapshot of Fig. 2). It becomes very irregular only towards the end of the dynamics (third snapshot of Fig. 2) when $p(t)$ is close to the percolation threshold p_c on the same lattice [9].

(ii) The ''active'' part of the global surface is essentially restricted the etching front, since a site having resisted the corrosion at a certain time step will resist forever.

These observations are useful for a first analysis of the dynamics. Roughly speaking, if the front advances linearly, the number of solid sites discovered at each time step is L (the number of sites in each layer). Hence, in this approximation, the number of etched sites is $n(t)=L\,p(t)$. Using this approximation one gets [from Eq. (2)]

$$p(t)=p(t-1)\left(1-\frac{L}{V}\right)=p(0)\left(1-\frac{L}{V}\right)^t. \tag{3}$$

This simple prediction is compared with the actual simulation behavior of $p(t)$ in Fig. 3. The agreement between the simple prediction 3 and the initial decay of $p(t)$ is very good for values $p(t)>p_c$, i.e., in the *smooth regime* of the dy-

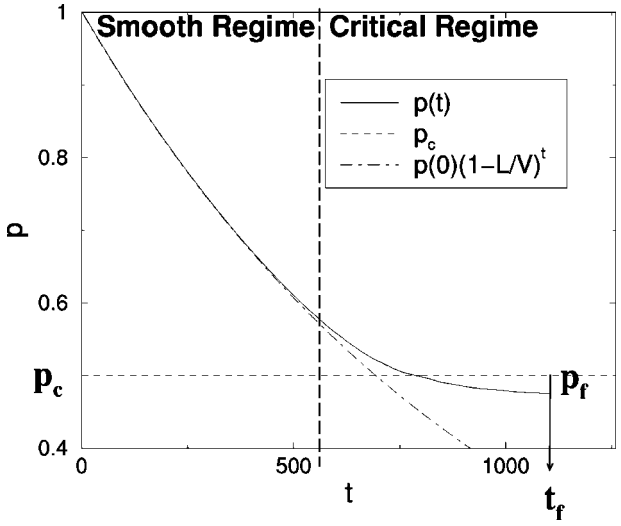

FIG. 3. Decay of the corroding power $p(t)$ in a triangular lattice with $p(0)=1$. The numerical evolution of $p(t)$ (solid line) is compared with the simple phenomenologic derivation of Eq. (3) (dashed line). When the two curves separate, the dynamics enters the ''critical regime'' dominated by percolation effects.

namics. When $p(t)$ is close to p_c, this approximation is no longer valid and the dynamics enters the *critical regime.*

A better derivation of Eq. (3), and a more precise definition of the two regimes, will be given below providing a deeper insight into the critical regime of the dynamics, when the surface becomes fractal and the dynamics slow down and stop.

Note that the main hypothesis for the derivation of Eq. (3) consists in assuming that at each time step the number of new sites checked for corrosion is always L, i.e., the whole next solid layer. This is possible if the etching does not leave large connected segments of uncorroded sites. In fact, it is easy to show that the nonetched sites, the number of which is approximatively $[1-p(t)]L$, are almost isolated, the average size of a segment of ''survived'' sites being $\langle l\rangle = 1/p(t)$.

Interestingly, the present phenomenological approach suggests an analogy between our dynamical etching model and a static percolation model known as gradient percolation [9,11]. This will be discussed next.

B. Analogy with gradient percolation (GP)

The gradient percolation (GP) problem [11,12] can be formulated in the following way: a random number $r_i \in [0,1]$ is assigned to each site of a lattice of x size L and y size h. A constant gradient of occupation probability in the y direction is then imposed on the lattice: $p(y)=1-y/h=1-y\,\nabla p$. The occupation rule is that in each column a site i is occupied if and only if $r_i<p(y)$ (see Fig. 4).

In the first column ($y=0$) the occupation probability is 1, while in the last one ($y=h$) it is zero. These two special layers individuate two percolating clusters in the x direction of occupied (gray) and empty (white) sites (Fig. 4). The external frontier of the connected occupied cluster is called the *gradient percolation front* [11]. This front is centered around the layer with $p(y)$ equal to the critical percolation threshold p_c characteristic of the lattice type. The front is fractal with a

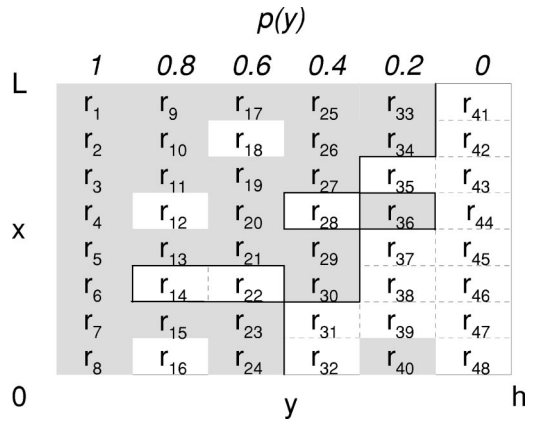

FIG. 4. The gradient percolation model. The numbers r are chosen randomly between 0 and 1. Each column has an occupation probability $p(y)$ ranging from 1 at the left side to 0 on the right side. A site i is occupied if $r_i<p(y)$. The occupied and empty sites are represented, respectively, in gray and white. Apart from isolated islands and lakes, gray and white sites form two distinct connected regions. The bold line represents the separation between these two regions.

dimension $D_f^{(\mathrm{GP})}\simeq 1.75$ up to a finite length (front width σ_{GP}) which is a power law of the local gradient $\nabla p=1/h$:

$$\sigma_{\mathrm{GP}} \sim [\nabla p]^{-\alpha_\sigma^{(\mathrm{GP})}}, \tag{4}$$

where $\alpha_\sigma^{(\mathrm{GP})}\simeq 0.57$. Note that $D_f^{(\mathrm{GP})}\simeq 7/4$ and $\alpha_\sigma^{(\mathrm{GP})} \simeq 1/D_f^{(\mathrm{GP})}$. For this reason it was assumed that D_f^{GP} is equal to the fractal dimension of the hull of the incipient infinite percolating cluster $D_f^h=7/4$ in percolation theory [13,18]. The demonstration of the identity of the equivalent of $\alpha_\sigma^{(\mathrm{GP})} = 1/D_f^{(\mathrm{GP})}$ in percolation theory is given in [13].

In addition, the occupation probabilities of the front range in an interval $p(y)\simeq p_c \pm \Delta p$, where Δp scales with the gradient as

$$\Delta p \sim [\nabla p]^{\alpha_p^{(\mathrm{GP})}}. \tag{5}$$

The exponent $\alpha_p^{(\mathrm{GP})}$ is related to $\alpha_\sigma^{(\mathrm{GP})}$, as $\Delta p \sim \sigma\,\nabla p$, which implies, from Eq. (4), $\alpha_p^{(\mathrm{GP})}=1-\alpha_\sigma^{(\mathrm{GP})}$.

Because of its characteristic properties, GP has provided a powerful method to compute percolation threshold p_c [14].

In this model, one can associate for each corroded site (x,y) the value $p(x,y)$ of the solution etching power at the time of corrosion of that site [9]. In this way, a position-dependent ''field'' of occupation probabilities (by the solution) is spontaneously generated. This is the physical link with GP. In the smooth time regime the successive active zones are consecutive solid layers containing about L sites. Consequently, $p(x,y)$ depends only on y [$p(x,y)=p(y)$].

The ''active'' zone at time t is then the whole layer at depth $y=t$. From Eq. (3) one can then write

$$p(y)=p(0)\left(1-\frac{L}{V}\right)^y. \tag{6}$$

This equation defines a *self-organized gradient percolation,* where the value of the gradient depends on the parameter L and V as

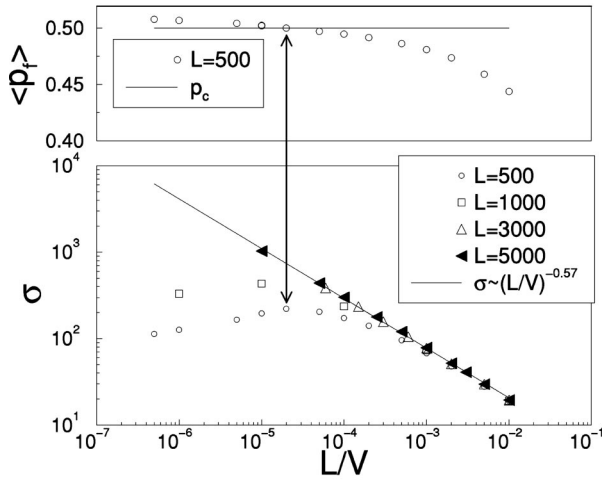

FIG. 5. Determination of the different corrosion behaviors. Bottom: behavior of σ as a function of L/V for several sample sizes (several values of L). Top: the behavior of $\langle p_f \rangle$ for the smaller sample ($L=500$). Note that the maximum of σ corresponds to the change of sign of $\langle p_f \rangle - p_c$ (vertical arrow).

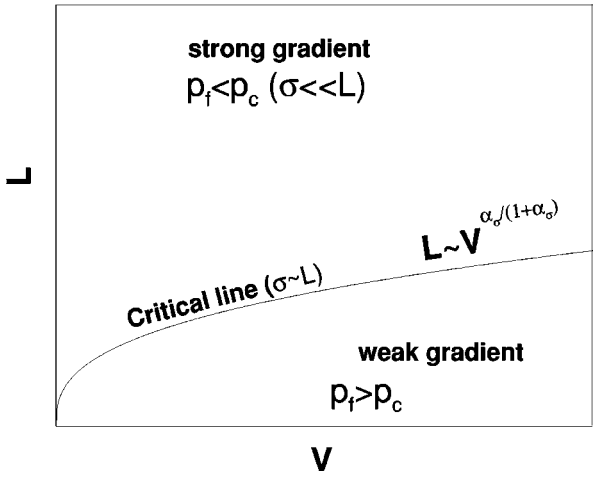

FIG. 6. ''Phase'' diagram in the parameters space (see text).

$$(\nabla p)_{\mathrm{et}} \sim \frac{L}{V}. \tag{7}$$

III. SIMULATIONS AND NUMERICAL RESULTS

Extensive simulations have been performed, considering triangular and square lattices, with first-nearest-neighbor (fnn) and second-nearest-neighbor (snn) (diagonal) connections for the corrosion process. All simulations start with $p_0=1>p_c$ in order to observe clearly the transition towards a critical regime, when $p(t)\simeq p_c$. Once p_0 is fixed, the parameter measuring the initial corroding ''force'' of the solution is $V=N_{\mathrm{et}}(0)/p_0$. The other fundamental parameter is the transversal size of the solid L. All the data presented below refer to 1000 different realizations of the quenched disorder, for each choice of the parameters L and V.

A. Correlation length and ''phase'' diagram

In order to quantify the statistical properties developed by the dynamical process, the average thickness of the final corrosion front is measured. If $\{y_i\}$ are the depths of the points i belonging to the corrosion front at time t, its average thickness can be defined as

$$\sigma = \sqrt{\frac{1}{I}\sum_{i=1}^{I} y_i^2 - \left(\frac{1}{I}\sum_{i=i,I} y_i\right)^2},$$

where I is the length of the corrosion front.

The behavior of the final value σ at time t_f as a function of the ''natural'' gradient L/V is shown in Fig. 5 (bottom) for different fixed values of L. Several observations can be made.

(i) First, for sufficiently large values of L/V (right side of Fig. 5), σ follows the scaling behavior

$$\sigma \sim (L/V)^{-\alpha_\sigma} \tag{8}$$

with $\alpha_\sigma = 0.57 \pm 0.02$. This confirms the idea that the final features of our dynamical etching model, at least in this range of L/V, are in the same universality class of GP once the identification $L/V \sim \nabla p$ is done, i.e., $\alpha_\sigma = \alpha_\sigma^{(\mathrm{GP})}$.

(ii) Decreasing L/V, σ increases following the previous scaling behavior [Eq. (8)] until reaching values of L/V for which $\sigma \simeq L$. For even smaller values of L/V, a deviation from the aforementioned scaling law is observed. This deviation is characterized by a crossover to a region dominated by boundary effects. In this regime σ seems to decrease slowly together with the gradient L/V, instead of increasing.

(iii) Consequently, for a fixed value of L, one can distinguish a ''strong gradient'' process, i.e., for values of L/V in which Eq. (8) holds, and a ''weak gradient'' process for values of L/V smaller than the crossover value. The crossover between the two behaviors is marked by a marginal value of L/V for which $\sigma \simeq L$. Note that for this value of L/V the spatial correlations extend all over the sample. Then this is a kind of ''critical''value of L/V.

Moreover one observes that $\langle p_f \rangle < p_c$ in the strong gradient regime and $\langle p_f \rangle > p_c$ in the weak gradient regime, where $\langle \cdots \rangle$ means an average over different realizations of the disorder with fixed parameters L,V. In this way the equality $\langle p_f \rangle = p_c$ can be used to identify the marginal (''critical'') value of L/V for a fixed value of L.

In the upper diagram of Fig. 5, the transition between the two regimes for $L=500$ is shown. This transition corresponds to a value of $L/V \simeq 2\times 10^{-5}$ (marked by the double arrow crossing the two plots).

This behavior of σ allows us to sketch a kind of ''phase'' diagram for our model in the (L,V) parameter space (Fig. 6). The ''critical'' line $\sigma \simeq L$ separates the two ''phases.'' Here we use the terminology of phase transitions because in GP the correlation length is equal to the front width σ.

Since in the strong gradient ''phase'' Eq. (8) holds, the scaling relation for the marginal line is

$$L \sim V^{\alpha_\sigma/1+\alpha_\sigma}. \tag{9}$$

The relevance of this relation with respect to the extensivity of spatial correlations in the ''thermodynamic limit'' is discussed in Appendix A. In the following, we deal only with

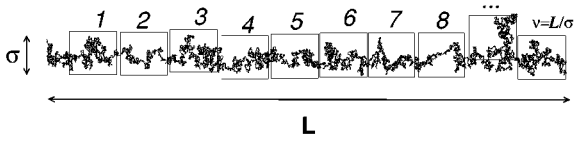

FIG. 7. Typical final corrosion front for a simulation in the strong gradient phase. Note that $\sigma \ll L$. Different nonoverlapping almost independent regions are identified by numbers. The number $\nu = L/\sigma$ of almost independent regions is relevant for the study of extremal quantities [15].

the strong gradient regime, leaving the detailed analysis of the weak gradient regime to further work.

B. Strong gradient etching

In order to study this regime, we focus on simulations of sizes $L = 3000$ and $L = 5000$, with $\langle p_f \rangle < p_c$. Such values of L are large enough, and at the same time they permit us to collect large statistics. A typical corrosion front is presented in Fig. 7, where the condition $L \gg \sigma$ is emphasized. Note that on scales larger than σ, the corrosion front is almost flat. This indicates the statistical independence among nonoverlapping regions of the surface of linear size larger than σ.

As mentioned earlier, σ is described by Eq. (8). Similar to σ, other important properties follow simple scaling relations with the gradient L/V [9].

The distance of the average value $\langle p_f \rangle$ from p_c follows the scaling law:

$$p_c - \langle p_f \rangle \sim \left(\frac{L}{V} \right)^{\alpha_p} \quad \text{with} \quad \alpha_p = 0.46 \pm 0.02 \tag{10}$$

as shown in Fig. 8. Appendix A discusses the possibility of obtaining a value of $\langle p_f \rangle$ arbitrarily near p_c, remaining in the ''strong gradient'' region of Fig. 6. Starting from a couple (L_0, V_0) in the strong gradient phase, one can obtain it, for instance, performing the limit $V \to \infty$ on any line $(L/L_0) = (V/V_0)^a$ with $\alpha_\sigma/(1+\alpha_\sigma) \leq a < 1$.

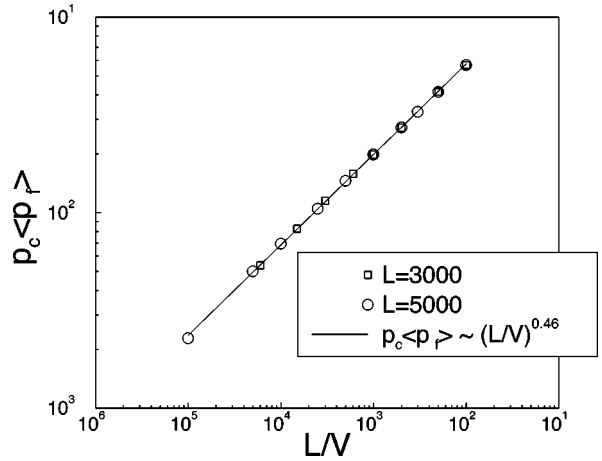

FIG. 8. Scaling behavior of $p_c - \langle p_f \rangle$. Note that, identifying L/V with ∇p of gradient percolation, one obtains the same values of the exponent $\alpha_p = 0.46 \pm 0.02$.

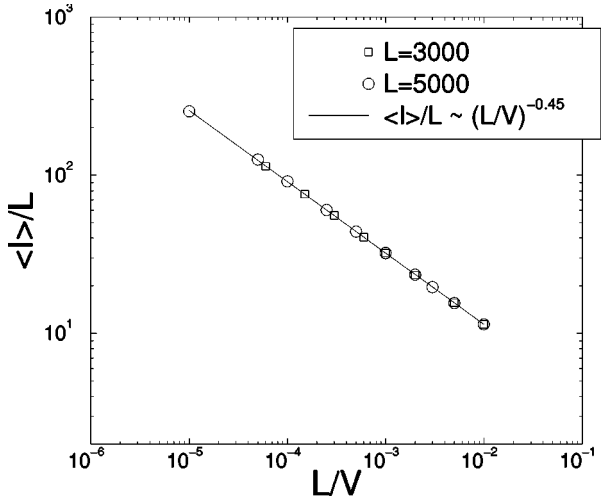

FIG. 9. Scaling behavior of the average number of sites per column in the final corrosion front.

Moreover, the average number of corrosion front sites per column (see Fig. 9) $\langle I(t_f) \rangle / L$ is found to follow a power law of the form

$$\frac{\langle I(t_f) \rangle}{L} \sim \left(\frac{L}{V} \right)^{-\alpha_I} \quad \text{with} \quad \alpha_I = 0.45 \pm 0.02. \tag{11}$$

The fractal dimension D_f of the corrosion front was measured (up to the scale σ) using the box-counting [16] algorithm. In this way $D_f = 1.753 \pm 0.005$ is found (see Fig. 10). Note that it is compatible with the value 7/4 of GP.

In the early papers about this etching process [9] $D_f \simeq 1.62$ was measured. This different value was due to finite-size effects. The present simulations are almost 400 times larger than those previously reported in [9] (the largest value of the parameters being $L = 3 \times 10^4$ and $V = 5 \times 10^9$). This achievement is important to assert that the exponents characterizing the final corrosion front belong to the universality class of gradient percolation. While $\langle p_f \rangle$ depends on the lattice geometry, as p_c changes, the values of the exponents remain the same.

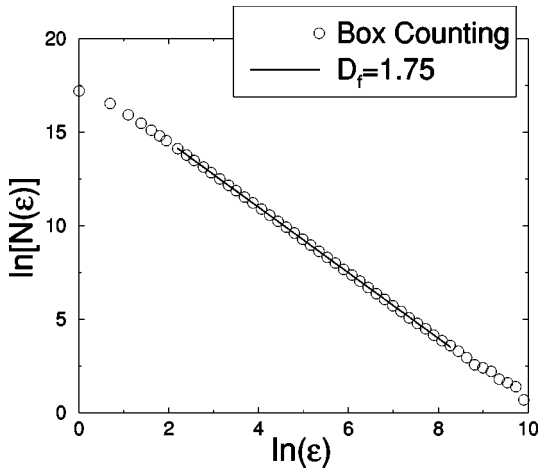

FIG. 10. Box-counting determination of the fractal dimension D_f of the corrosion front. The value of $D_f = 1.753 \pm 0.005$ is found fitting for values of ϵ ranging from a few lattice distances to the front width σ [in this case $\sigma \approx 3000$, i.e., $\ln(\sigma) \approx 8$].

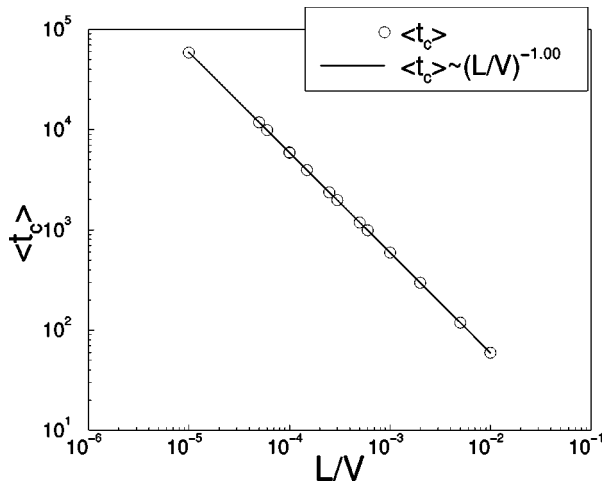

FIG. 11. Scaling behavior of the critical time t_c for which $p(t_c)=p_c$: $\langle t_c\rangle \sim (L/V)^{-\alpha_{t_c}}$ with $\alpha_{t_c}=0.998\pm0.001$.

Nevertheless, note that the measured fractal dimension of the corrosion front can be reduced to $\frac{4}{3}$, if one does not use the right ''dual'' connectivity criterion introduced above. This is the so-called Grossmann-Aharony effect in percolation [12,17]. This effect can explain the reduced fractal dimension (4/3) measured in the real corrosion experiments [7], due to insufficient image resolution. For example, on the triangular lattice (where the solution etches only fnn), if the resolution does not distinguish first and second nearest neighbors, the measured fractal dimension is 4/3.

The average critical time t_c, defined by $p(t_c)=p_c$, and the difference between the arrest time t_f of the dynamics and t_c itself, are measured for different values of the gradient L/V. For the first one, the following simple behavior is found (see Fig. 11):

$$\langle t_c\rangle \sim (L/V)^{-\alpha_{t_c}} \quad \text{with} \quad \alpha_{t_c}=0.998\pm0.001. \tag{12}$$

As we shall see in the following, this is a direct consequence of the linear properties of the smooth dynamical regime [Eq. (3)].

Finally, for t_f one has (see Fig. 12)

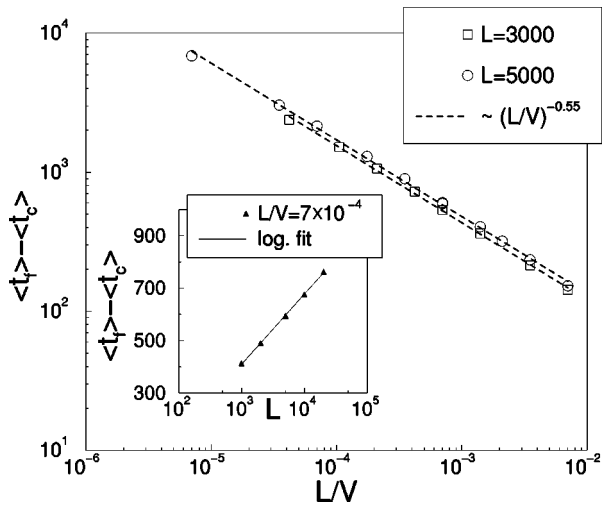

FIG. 12. Scaling behavior of $\langle t_f\rangle-\langle t_c\rangle$ for different values of L. Inset: the dependence on L for L/V fixed is presented.

$$\langle t_f\rangle-\langle t_c\rangle \sim (L/V)^{-\alpha_{t_f}} \quad \text{with} \quad \alpha_{t_f}\approx 0.55. \tag{13}$$

However, for $\langle t_f\rangle-\langle t_c\rangle$, a further dependence on L is obtained (see the inset of Fig. 12). In particular, changing L with L/V fixed, the quantity $\langle t_f\rangle-\langle t_c\rangle$ is found to depend linearly on $\ln L$. This behavior is connected to the ''extremal'' nature of t_f and is not studied here [15].

C. Scaling relations

The exponents α_σ, α_p, α_I, and D_f are not independent. At first, note that, within the present numerical precision,

$$\alpha_\sigma=\frac{1}{D_f} \tag{14}$$

as in GP [11].

Identifying the width σ with the horizontal correlation length, the average number within a correlated region scales as σ^{D_f} because of the fractality on smaller scales. Since the horizontal size of the solid is L, the average number of distinct correlated regions will be L/σ. Consequently, one can write

$$\langle I(t_f)\rangle \sim \frac{L}{\sigma}\sigma^{D_f},$$

which implies

$$\frac{\langle I(t_f)\rangle}{L}\sim \sigma^{D_f-1}\sim\left(\frac{L}{V}\right)^{-\alpha_\sigma(D_f-1)}. \tag{15}$$

From Eqs. (11), (14), and (15) one then obtains the following scaling relation:

$$\alpha_I=\alpha_\sigma(D_f-1)=\frac{D_f-1}{D_f}, \tag{16}$$

which is consistent with the measurement of α_I in Eq. (11).

Exploiting the analogy between L/V and the gradient ∇p in GP, another interesting relation among exponents can be derived. From the relation $\Delta p\equiv p_c-p_f\approx\nabla p\cdot\sigma$, one gets

$$\alpha_p=1-\alpha_\sigma=\frac{D_f-1}{D_f}. \tag{17}$$

Note that this implies $\alpha_p=\alpha_I$ in $d=2$. In fact, the assumption that the number of different correlated regions scales as L/σ is valid only in $d=2$.

IV. DYNAMICAL EQUATIONS AND THEORETICAL RESULTS

In this section we present an analytical derivation of the dynamical evolution of $p(t)$ and the distribution of the surface resistances. This time-dependent distribution characterizes the evolution of ''hardening'' properties of the surface. To this aim, the histogram $h(r,t)$ is introduced. The quantity $h(r,t)dr$ measures the number of global surface sites with random resistance in the interval $[r,r+dr]$ at time t. By definition, the number of sites in the global surface $G(t)$ is

simply the total integral of the histogram:

$$G(t)=\int_0^1 h(r,t)dr. \tag{18}$$

On the other side, the number of surface sites being corroded at time t by the solution will be

$$n(t)=\int_0^{p(t)} h(r,t)dr, \tag{19}$$

as $n(t)$ is the number of sites in the global surface with $r<p(t)$. Note that Eq. (19) links $h(r,t)$ directly to $p(t)$ through Eq. (2), which can then be rewritten as

$$p(t+1)=p(t)-\frac{\int_0^{p(t)} h(r,t)dr}{V}. \tag{20}$$

Let us call $m(t)$ the number of active sites at time $t+1$: i.e., the new sites entering the global surface as a consequence of the corrosion of the set of $n(t)$ sites. Then the set $m(t)$ is the *active zone* at time $t+1$. One can define $\omega(t)=m(t)/n(t)$. Therefore, $\omega(t)$ is the number of new active sites per etched site at time t. As shown below, the quantity $\omega(t)$ is the fundamental parameter relating the ''geometry'' to the ''chemistry'' of the system at time t. At each time step one can write

$$G(t+1)=G(t)-n(t)+m(t), \tag{21}$$

or, using both Eq. (19) and the definition of $\omega(t)$,

$$G(t+1)=G(t)+[\omega(t)-1]\int_0^{p(t)} h(r,t)dr. \tag{22}$$

Considering only sites in $[r,r+dr]$, one can write

$$h(r,t+1)=h(r,t)-h(r,t)\theta[p(t)-r]+\omega(t)\int_0^{p(t)} h(r',t)dr', \tag{23}$$

where $\theta(x)$ is the Heavyside step function. In Eq. (23), the second term on the right-hand side represents the number of sites etched at time t [a surface site i is etched with probability 1 if $r_i<p(t)$]. The third term is the contribution to $h(r,t)$ due to the new active zone. It is based on the fact that each new site has completely random resistance to etching; the probability that it belongs to the interval $[r,r+dr]$ is simply dr [as $\pi_0(r)=1$]. In principle, knowing the behavior of $\omega(t)$, one can solve the system given by Eqs. (20) and (23), characterizing in this way the dynamical evolution of the corrosion power and of the resistance of the solid surface.

Before going on with calculations, it is important to observe that $h(r,0)=L \quad \forall r\in[0,1]$ [as $\pi_0(r)=1$ and the initial surface is a layer of sites of length L]. On the other hand, for $r<p(t)$, Eq. (23) reduces to

$$h(r,t+1)=\omega(t)\int_0^{p(t)} h(r',t)dr'. \tag{24}$$

Equation (24) and the initial condition $h(r,0)=L$ imply that at each time for $r<p(t-1)$, $h(r,t)$ is independent of r and can be written as

$$h(r,t)=L\prod_{t'=0}^{t-1}(\omega(t')p(t')) \quad \text{for} \quad r<p(t-1). \tag{25}$$

Using this expression in Eq. (20), the following equation is obtained:

$$p(t+1)=p(t)\left[1-\frac{L}{V}\prod_{t'=0}^{t-1}(\omega(t')p(t'))\right]. \tag{26}$$

Equation (26) makes evident the strong dynamical link between the geometry $[\omega(t)]$ and the chemistry $[p(t)]$ of the system.

In order to examine the calculations further, it is necessary to make some hypotheses on the behavior of $\omega(t)$.

As previously mentioned, the dynamical evolutions can be divided into two regimes: (i) a first *smooth regime*, which is referred to the time scale at which $p(t)$ is larger than p_c; (ii) a second *critical regime*, which is referred to the time scale at which $p(t)\simeq p_c$.

This partition of the dynamics into two regimes is directly connected to percolation theory [10], as shown below.

A. Smooth regime

If one considers all the lattice sites with $r<p(t)$ for $p(t)>p_c$, they form both a set of a few finite-size clusters and an infinite percolating and homogeneous (not fractal) cluster [10]. Consequently, the intersection between the global solid-solution surface and this set is made of a large number of sites. The larger $p(t)$, the larger the intersection. This intersection is merely the set of $n(t)$ sites to be dissolved at that time step.

Since $n(t)\gg 1$ [and then $m(t-1)>n(t)\gg 1$ also], one can use the law of large numbers to relate $n(t)$ to $m(t-1)$:

$$n(t)=p(t)m(t-1). \tag{27}$$

For the same reason one expects small fluctuations around these values. From Eq. (27) and the definition of $\omega(t)$, one obtains

$$m(t)=\omega(t)p(t)m(t-1). \tag{28}$$

Because of the percolation properties for $p>p_c$, which are related to the previous argument, one expects

$$\left|\frac{m(t)-m(t-1)}{m(t-1)}\right|\ll 1.$$

Hence we obtain the relation

$$\omega(t)\simeq\frac{1}{p(t)}. \tag{29}$$

This equation introduces an important relationship between the fundamental ''chemical'' parameter $p(t)$ and the ''geo-

metrical'' and ''dynamical'' parameter $\omega(t)$. Inserting Eq. (29) into Eq. (26), one recovers Eq. (3), which can be rewritten as

$$p(t)=p(0)\exp\left(-\frac{t}{\tau}\right) \tag{30}$$

with $\tau=-1/\ln(1-L/V)\simeq V/L$ $(L\gg V)$. From Eq. (30) one has $t_c\simeq V/L\ \ln(p_0/p_c)\sim(L/V)^{-1}$. This confirms the numerical result found in Fig. 11 and expressed by Eq. (12). Note that the behavior given by Eq. (30) is independent of the space dimension and of the coordination number of the lattice. This behavior is, however, valid only up to the time at which $p(t)\simeq p_c$. After this time the hypothesis to deduce Eq. (30), and in particular the possibility of using the law of large numbers, breaks because of the geometrical constraints given by the percolation properties of random numbers on a lattice.

Using Eq. (30), one can derive rigorously the shape of $h(r,t)$ at any time step t or of its normalized version $\phi(r,t)$ [i.e., $\int_0^1 dr\ \phi(r,t)=1$]. $\phi(r,t)$ is obtained by dividing $h(r,t)$ by $G(t)$. Technical calculations are reported in Appendix B. We provide here directly the result

$$\phi(r,t)\simeq\phi_1(t)\times\begin{cases}\dfrac{1}{t} & \text{for } r\leqslant p(t)\\[2mm] 1-\dfrac{\tau}{t}[\ln p(0)-\ln r] & \text{for } p(t)\leqslant r\leqslant p(0)\\[2mm] 1 & \text{for } r\geqslant p(0),\end{cases} \tag{31}$$

where

$$[\phi_1(t)]^{-1}=1+[p(0)-p(t)]/\ln(p(t)/p(0))=1-\frac{\tau}{t}p(0)[1-\exp(-t/\tau)]. \tag{32}$$

Equation (31) can be rewritten, in terms of $p(t)$ instead of t, as follows:

$$\phi(r,t)\simeq\phi_1(t)\times\begin{cases}\dfrac{1}{t} & \text{for } r\leqslant p(t)\\[2mm] 1-\dfrac{\ln(r/p(0))}{\ln(p(t)/p(0))} & \text{for } p(t)\leqslant r\leqslant p(0)\\[2mm] 1 & \text{for } r\geqslant p(0).\end{cases} \tag{33}$$

B. Critical regime

For $p(t)=p_c$, one has (in the limit $L\to\infty$) a marginal critical case in which the set of lattice sites with $r<p(t)$ form finite-size clusters of any size and an infinite fractal percolating cluster. Finally for $p(t)<p_c$, the set of lattice sites with $r<p(t)$ forms only finite-size clusters. For this reason, even if at such time t the intersection between the global solid surface and the set of lattice sites with $r<p(t)$ is not empty, it becomes depleted after a finite number of time steps. The average number of time steps after which the dynamics stops will be a function of the system parameters L and V [Eq. (13)]. At this time the corrosion dynamics stops because the intersection between the global surface and the set of lattice sites with $r<p(t)$ is empty. This explains why the final corrosion front is fractal with a fractal dimension D_f and a characteristic size (thickness) σ. $D_f=\frac{7}{4}$ is the hull fractal dimension of the finite clusters formed by the lattice sites with $r<p(t_f)$ and σ is the characteristic size of these clusters. Finally, the same argument explains why each exponent, characterizing the above introduced scaling relations (apart from those about t_c and t_f), is directly connected to the exponents of GP.

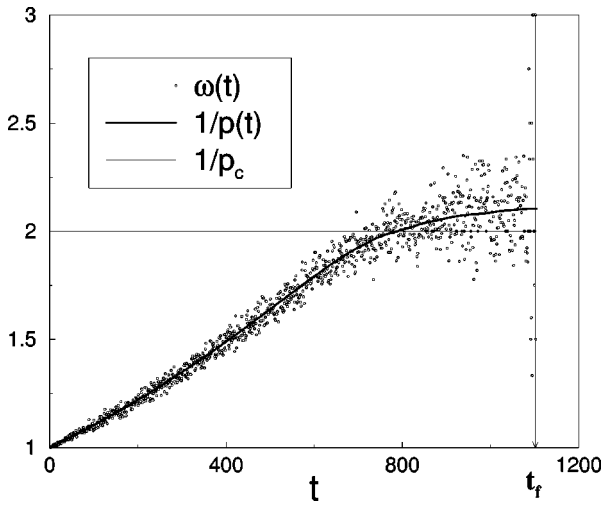

FIG. 13. Comparison between $\omega(t)$ (dots) and $1/p(t)$ (thick line) as functions of time.

From the above argument, it is important to note that, if not empty, the active zone at a time $t>t_c$ is composed of a small and fluctuating number of sites $m(t)$. This implies that also $n(t)$ is small and strongly fluctuating. Consequently, the arguments developed in dealing with the smooth time regime, based on the law of large numbers and small fluctuations, are no longer valid: $\omega(t)$ becomes a strongly fluctuating quantity. These critical fluctuations are related to the fractal morphology of the critical phase of percolation. We can say that the arrest of the etching dynamics is due to one of these big fluctuations of ω in which no site of the active zone has $r<p(t)$.

All these features are shown in Fig. 13, where $\omega(t)$ and $1/p(t)$ are shown as functions of time. It is important to note that, whereas $\omega(t)$ is a strong fluctuating quantity in the critical time regime, $p(t)$ is always smooth. In fact, $p(t)$ can be written [Eq. (2)] as

$$p(t)=p(0)-\frac{1}{V}\sum_{k=0}^{t-1}n(t).$$

Consequently, $p(t)$ can be seen, apart from prefactors, as the time integral of $n(t)$, which is a limited function of time and then $p(t)$ is continuous. Moreover, Fig. 13 shows that in the critical time regime the equality $\omega(t)\simeq 1/p(t)$ is valid only ''in average:''

$$\overline{\omega(t)} \simeq \frac{1}{p(t)}, \tag{34}$$

where $\overline{\omega(t)}$ means the average of ω over a sufficiently large time interval around t in the critical time regime. In order to justify the smooth behavior of $p(t)$ in spite of the fluctuations of $\omega(t)$, one can use Eq. (26). In the continuous time limit, it can be rewritten as

$$\frac{dp(t)}{dt} = -\frac{L}{V} p(t) \exp\left[\int_0^t dt' [\ln p(t') + \ln \omega(t')] \right]. \tag{35}$$

Since the fluctuating $\omega(t)$ appears in the integral term of the exponential of the right-hand side of Eq. (35), one expects $p(t)$ to be regular.

In order to understand why one has $\overline{\omega(t)} \simeq 1/p(t)$ also in the critical regime, one has to analyze the behavior of time average,

$$\overline{\omega(t)} \equiv \frac{1}{\Delta t} \sum_{t'=t-\Delta t/2}^{t+\Delta t/2} \omega(t').$$

Using the definition of $\omega(t)$, one can write

$$\overline{\omega(t)} = \frac{1}{\Delta t} \sum_{t'=t-\Delta t/2}^{t+\Delta t/2} \left[\frac{m(t'-1)}{n(t')} \frac{m(t')}{m(t'-1)} \right]. \tag{36}$$

From Eq. (27) one has directly

$$\sum_{t'=t-\Delta t/2'}^{t+\Delta t/2} [m(t'-1)/n(t')] = 1/p(t).$$

From this observation and supposing that the quantity $m(t')/m(t'-1)$ oscillates symmetrically around 1, one expects Eq. (34). Before proceeding, it is worth noting that the variation of $p(t)$ during the critical time regime, as shown by Eq. (10), is very small. From this one has approximatively

$$\overline{\omega(t)} \simeq 1/p_c. \tag{37}$$

Equations (34) and (37) are very important because they provide both a ''physical'' and a ''geometrical'' meaning to the critical threshold of percolation in a given lattice (an analogous relation for invasion percolation was found in [18,19]).

In order to clarify the geometrical effect on $\omega(t)$, it is important to observe that, following Eq. (29) and Eq. (30), $\omega(t)$ would increase to infinity. Clearly this is not possible in a finite dimensional lattice with a finite coordination number. For instance, in a $2d$ site square lattice with fnn connection, ω must always be smaller than 3. Moreover, as seen above, the percolation theory introduces a stronger constraint forbidding $p(t)$ to go well below p_c. Note that p_c is always larger than the inverse of the coordination number of the lattice [10]. They are equal only in the Bethe lattice without loops. Consequently, in order to use Eq. (26) to predict the behavior of $p(t)$, one has to take into account both the behavior given by Eq. (34) and these geometrical constraints. In order to show this, we have made the approximation $\omega(t) = 1/p_{\rm sim}(t)$ in Eq. (26), where $p_{\rm sim}(t)$ is the simulation outcome for $p(t)$ (and then it includes automatically the geometrical constraint). The solution $p(t)$ obtained by solving numerically Eq. (26) is very near to $p_{\rm sim}(t)$ itself.

Because of the strong fluctuations, the purely analytical study of this critical regime is difficult. For this reason we developed only an approximated mean-field approach by imposing only the geometrical constraint with the following simple approximation:

$$\omega(t) = 1/p_c \tag{38}$$

in this critical time regime. This is a kind of mean-field approximation as the fluctuations of $\omega(t)$ are neglected. Inserting the relation (38) into Eq. (26), one can write

$$p(t+1) = p(t) \left[1 - \frac{L}{V} p_c^{-t} \prod_{t'=0}^{t-1} p(t') \right] \tag{39}$$

with the initial condition $p(t_c) = p_c$ and $t > t_c$. In order to solve Eq. (39), one can consider the continuous limit which is equivalent to taking $\omega(t) = 1/p_c$ in Eq. (35):

$$\frac{dp(t)}{dt} = -\frac{L}{V} p(t) \exp\left[\int_0^t dt' \left(\ln \frac{p(t')}{p_c} \right) \right]. \tag{40}$$

This equation can be solved exactly, and this solution is well approximated by

$$p_c - p(t) \simeq p_c \sqrt{\frac{2L}{V}} \frac{\exp\left(\sqrt{\frac{2L}{V}} (t - t_c) \right) - 1}{\exp\left(\sqrt{\frac{2L}{V}} (t - t_c) \right) + 1}, \tag{41}$$

where t_c is the time at which $p(t) = p_c$. From Eq. (41) we can see that in the $t \to \infty$ limit one has

$$p_c - p_f \sim \sqrt{\frac{L}{V}}. \tag{42}$$

In spite of the rough approximation, we obtain a good approximation of the numerical result of Eq. (10) (see also Fig. 8), therefore this ''mean-field'' result provides a good approximation.

Moreover, since the time constant of Eq. (41) is $\tau' \sim \sqrt{V/L}$, it is argued that the average time t_f at which the dynamics spontaneously stop obeys the following scaling law:

$$t_f - t_c \sim \tau' \sim \sqrt{\frac{V}{L}}.$$

Also, this is a reasonable approximation with respect to the simulation behavior [Eq. (13) and Fig. 12]. We can see that Eq. (42) can be interpreted as the product of the Δp in single time steps ($\Delta p \sim L/V$) multiplied by the average number of time steps necessary to stop the dynamics $t_f - t_c \sim \sqrt{V/L}$.

V. FINAL HISTOGRAMS AND SURFACE HARDENING

The surface hardening can be described by considering both the histogram of the global surface and that of the cor-

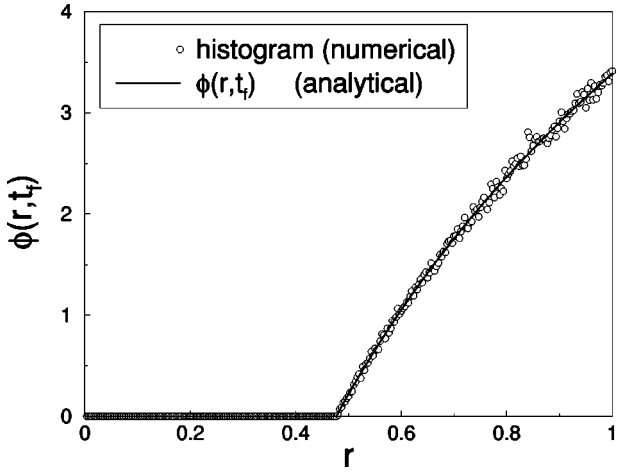

FIG. 14. Normalized histogram of site resistances belonging to the final global surface. Circles represent the result of numerical simulations and the solid line the theoretical prediction detailed in Appendix B.

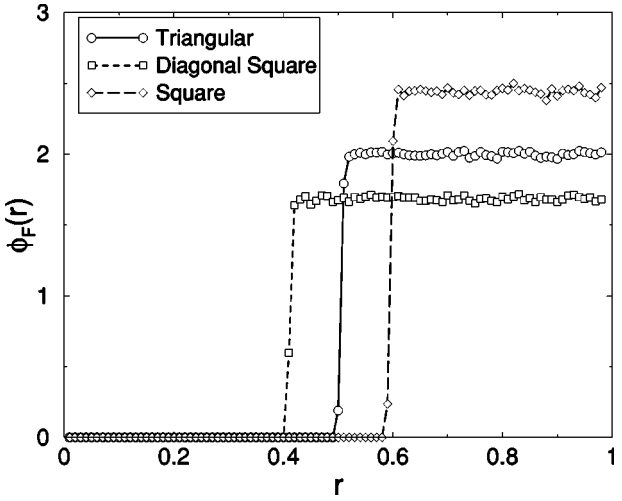

FIG. 15. Normalized histogram of the corrosion front resistances. One can notice that simple step functions are found for any three different lattices studied. The discontinuities occur very near the percolation thresholds.

rosion front. One first observes that the number of corroded sites in the critical regime is much smaller than the number of sites which have been etched in the smooth regime. This means that the global surface is dominated by sites belonging to finite clusters. As a consequence, $\phi(r,t_f)$ is well approximated by the linear regime behavior given in Eq. (B7) with $t=t_f$ and $p(t)=p_f$ (see Fig. 14).

One observes good agreement between theory and numerics.

The global histogram describes the hardening phenomenon of the global surface which includes finite-size clusters detached by the etching process at various time steps of the dynamics. The increasing behavior of $\phi(r,t_f)$ for $r>p_c$ is due to the fact that the majority of surface sites belonging to finite islands have been discovered at intermediate time steps when $p(t)>p_c$. This implies that their resistance is well above p_c.

The hardening of the corrosion front is described by the normalized distribution $\phi_F(r)$ of site resistances. It has been measured by numerical simulation for several types of lattices. The numerical results are shown in Fig. 15.

As discussed above, the final front is more resistant to etching than the original native surface. This is shown in Fig. 15, giving the histogram of the front resistances. In first approximation it is a step function around $r=p_c$. This confirms the hypothesis, derived by GP, that the final corrosion front corresponds to the hull of percolation clusters with $p=p_f$.

This effect could possibly be used practically in waste management problems. Consider, for instance, a system containing dangerous compounds with random resistances to etchants present in the environment. If in natural circumstances it comes in contact with etchants, even with a weak etching power $p_0<p_c$, then dangerous materials can be diffused in the environment.

But one can think to apply to the system a previous etching treatment with $p_0'>p_c$, in an artificially controlled situation. In this case the final surface contains only sites with $r>p_c$. Then the treated surface will resist forever any further natural attack with $p<p_c$, with no danger of leaks in nature. This could be called a random ''Darwinian'' selection of a strong surface: once selected with a finite solution with $p>p_c$, the surface resists for ever further etching with $p_0<p_c$ whatever the volume of the solution.

VI. DISCUSSION

Several properties and limitations of this model should be discussed. This depends on the nature of what has been described here as a ''site.'' One can think of a site as being an atom or a small group of atoms. For example, if one considers a random solid (such as a glass), the different local random environments will cause random local rates for atomic dissolution rather than random probabilities. The possible application of the above model is then restricted to situations where the choice of suitable time intervals makes it possible to separate ''very resistant'' and ''very weak'' sites. This implies a transposition of the distribution of local rates into a distribution of site resistances.

But a site could also be a semimacroscopic entity like a small crystallite protected by a randomly resistive surface. In the case of corrosion experiments by Balàzs [8], it is believed that randomness may be attributed to the random nature of the oxide layer which spontaneously grows on previously etched aluminum crystallites. The disorder studied herein occurs if the random resistances to etching appear just after oxidation of newly discovered crystallites. Although the disorder appears dynamically, once created it is quenched.

It is worth noting that a different kind of process would lead to the same description. Consider, for example, a case where crystallite oxidation and corrosion are two possible processes in competition when a site is uncovered. If the probability p associated to the corrosion is proportional to the global etchant concentration, then a probability $1-p$ should be associated to oxidation (and then passivation). In order to decide the etching or passivation of a given site i, a random number r_i is thrown. If r_i is smaller than p, the site is corroded, otherwise it is defintively passivated. The r_i numbers define a stochastic process which would give the

same dynamical behavior. Of course the hardening properties would be different in that case. From a statistical point of view, it means simply that we can equivalently formulate our model as a deterministic dynamics with quenched disorder or as a stochastic dynamics without quenched randomness.

VII. CONCLUSIONS

In this paper we have discussed several aspects of a simple model for the etching of a two-dimensional disordered system by a finite volume of corroding solution. This has been done both theoretically and verified numerically. The dynamics correspond to the disappearance of weak surface sites which at the same time uncovers new sites. As the etching process consumes the etchant, the etching power of the solution decreases and the surface resistance increases to the point where the process stops spontaneously. One obtains a kind of ''equilibrium'' or static situation in which the dynamics is stopped. This static state is characterized by the fact that the surviving interface sites have a resistance to the etching which is larger than the final value p_f of the solution etching power which is on the order of the percolation threshold p_c.

An analytical description of the time behavior of the solution etching power $p(t)$ and of the distribution of resistances on the total interface has been introduced. This analytical approach indicates why and how the dynamics can be divided into two regimes. The first initial period corresponds to a classical, or superuniversal, regime. It can be described with precision by a mean-field approximation. The second regime is a critical regime related to percolation criticality. The final connected interface is constituted by a collection of fractal interfaces up to a certain characteristic depth or scale σ. The fractal dimension is found to be very close to $D_f = 7/4$. The difference $p_c - p_f$ between p_c and the final etching power p_f and the width σ are both linked to the geometrical and external parameters characterizing the system via simple scaling relations. These properties can be simply explained by relating the model to the gradient percolation model: identifying the ratio L/V between the size of the solid and the volume of the solution with the gradient ∇p which characterizes the scaling properties of GP. After this identification, it has been shown that our etching model belongs to the GP universality class, and that the exponents can be explained through percolation theory.

An important result of this approach is the identification of the meaning of $p(t)$ as the inverse of the mean number of new interface sites uncovered by each etched site. This identification in particular is very important in relation to the static final situation in which $p(t) \simeq p_c$, as it provides the physical meaning of the percolation critical threshold.

Several further developments of these studies can be suggested. The statistics of other observable quantities, such as the arrest time of the process t_f or the maximal depth attained by the solution, can be studied and related to known results of asymptotic extreme theory [15]. In particular, such statistics determine the probability of ''chemical'' fracture of a finite solid submitted to an etching process. Furthermore, the distribution of the debris produced by the etching process can be regarded as a ''chemical'' fragmentation process.

Also, the stability of the final (harder) interface with respect to external perturbations (as, for example, fluctuation of the etching power p_f) should be of interest.

ACKNOWLEDGMENTS

The authors would like to acknowledge M. Filoche and M. Dejmek for interesting discussions and a critical reading of the manuscript. This work has been supported by the European Community TMR Network ''Fractal Structures and Self-Organization'' ERBFMRXCT980183. The ''Laboratoire de Physique de la Matière Condensée de l'Ecole Polytechnique'' and the ''Center de Mathématiques et de leurs Applications de l'Ecole Normale Superieure de Cachan'' are '' Unités mixtes de recherches du CNRS'' under the respective numbers 7453 and 8536.

APPENDIX A: THERMODYNAMIC LIMIT

In light of what was written about the ''phase'' diagram, one can discuss the thermodynamic limit. Let us start with a couple of external parameters (L_0, V_0) in the strong gradient ''phase'' for which $\sigma(L_0, V_0) \ll L_0$, and negligible boundary effects. If one changes L (horizontal size of the solid) and V (volume of the solution) by satisfying the relation

$$\frac{L}{L_0} = \left(\frac{V}{V_0}\right)^{\alpha_\sigma/1+\alpha_\sigma},$$

the new system remains in the strong gradient ''phase'' for any value of V. The final corrosion front obeys the relation

$$\frac{\sigma(L,V)}{L} = \frac{\sigma(L_0,V_0)}{L_0},$$

i.e., the new system is geometrically ''similar'' to the old one.

Let us now study what happens changing (L,V) following the relation

$$\frac{L}{L_0} = \left(\frac{V}{V_0}\right)^{a} \tag{A1}$$

with $a \neq \alpha_\sigma/(1+\alpha_\sigma)$.

(i) If $a > 1$, the system stays in the strong gradient phase for any value of V, but $\sigma(L,V)$ is a decreasing function of V and in the thermodynamic limit $(V \to \infty)$, the final corrosion front is ''microscopically'' flat.

(ii) If $\alpha_\sigma/(1+\alpha_\sigma) < a \leqslant 1$, the system stays in the strong gradient phase. Moreover, $\sigma(L,V)$ increases with V (it is infinite in the thermodynamic limit), but $\sigma(L,V)/L < \sigma(L_0,V_0)/L_0$. Hence the new corrosion front is not ''similar'' to the old one, and in the limit $V \to \infty$ it becomes ''macroscopically'' flat.

(iii) If $a < \alpha_\sigma/(1+\alpha_\sigma)$, $\sigma(L,V)/L$ increases with V. However, there will be a marginal (or ''critical'') value V_c of the volume for which the geometric correlations reach their maximum possible value: $\sigma(L,V) \simeq L$. Increasing V further, following Eq. (A1), the system enters the weak gradient phase dominated by boundary effects.

APPENDIX B: THE ''GLOBAL'' HISTOGRAM

In the smooth regime, at each time step t, the number of surface sites which are created is L, and the number of dissolved sites is $p(t)L$. Consequently, at each time step, the total number of surface sites increases by $[1-p(t)]L$. More precisely, we can see that these last sites affect only the high r part of the histogram. In fact, using Eq. (25) in Eq. (23), one can write the explicit form of $h(r,t)$ for any time step in the smooth regime:

$$h(r,t) = \begin{cases} L & \text{for } r<p(t-1) \\ \dots & \\ (t-t')L & \text{for } p(t'+1)<r\leqslant p(t');\ t'\leqslant t-2 \\ \dots & \\ (t+1)L & \text{for } r>p(0). \end{cases} \tag{B1}$$

Note that $h(r,t)$ is, at any time, a nondecreasing multistep function of r. Each step differs from the previous one by height L.

It can be written also

$$h(r,t)=L\,\theta(p(t-1)-r)+\sum_{t'=0}^{t-2}[(t-t')L\,\theta(r-p(t'+1)) \times\theta(p(t')-r)]+(t+1)L\,\theta(r-p(0)). \tag{B2}$$

In a similar way, the explicit function $G(t)$ is obtained by inserting Eq. (25) and Eq. (30) in Eq. (22):

$$G(t)=L\left[t+1-p(0)\frac{1-\exp\left(-\frac{t}{\tau}\right)}{1-\exp\left(-\frac{1}{\tau}\right)}\right]. \tag{B3}$$

In order to obtain the normalized histogram $\phi(r,t)$, one has to divide Eq. (B1) by Eq. (B3). Because of the steplike shape of Eq. (B1), $\phi(r,t)$ will also be steplike.

A more physical derivation of a smooth function interpolating the steplike $\phi(r,t)$ can be obtained under the same approximate phenomenological approach leading to Eq. (3). Under these assumptions, the corrosion front is located at depth y at the time $t=y$ when the solution has the corrosive power $p(t=y)$, where $p(t)$ is given by Eq. (3) [or alternatively by Eq. (30)]. From Eq. (3), one can deduce that the solution attains the etching power p at the time $t(p)$ given by

$$t(p)=\frac{\ln(p/p(0))}{\ln(1-L/V)} \tag{B4}$$

when the front is at depth $y=t(p)$. From this equation, it is possible to infer that a site with random resistance $p(0)<r<p(t)$ is etched only if it is located at a depth $y<t(r)$. In fact, if $y>t(r)$, the site would be reached by the solution (i.e., checked by the dynamics) when the etching power $p(t)$ is weaker than its resistance r. Hence, it is necessary to distinguish three cases, in order to write the number of solid sites, with resistance in $[r,r+dr]$, belonging to the global surface at time t.

(i) All the sites with $r>p(0)$ checked by the dynamics resisted the corrosion, and hence belong to the surface. Their number is given by dr multiplied by the area spanned by the front up to time $t-1$ (included), in addition to such sites on the corrosion front at time t: $(L\,t+L)dr$.

(ii) All the sites with $p(t)<r<p(0)$ checked by the dynamics before time $t(r)$ have been etched, whereas such sites checked between $t(r)$ and t resisted. The number is given by dr multiplied by the area spanned by the front between times $t(r)$ and $t-1$ (included), in addition to the sites on the front at time t: $\{L[t-t(r)]+L\}dr$.

(iii) All the sites with $r<p(t)$ checked by the dynamics have been etched. Only sites with such resistence belonging to the corrosion front at time t contribute to the histogram. Their number is $L\,dr$.

One can then write

$$h(r,t)=\begin{cases} L & \text{for } r\leqslant p(t) \\ L[t-t(r)+1] & \text{for } p(t)\leqslant r\leqslant p(0) \\ L(t+1) & \text{for } r\geqslant p(0). \end{cases} \tag{B5}$$

Using the explicit formula for $t(r)$ given by Eq. (B4), with r replacing p, one has

$$G(t)=\int_0^1 h(r,t)dr=L[t+1-\tau p(0)(1-e^{-t/\tau})], \tag{B6}$$

where $\tau=[\ln(1/L/V)]^{-1}\simeq V/L$. Note that Eq. (B6) differs from the rigorous Eq. (B3) only from the approximation $\exp(-1/\tau)\simeq 1-1/\tau$, which is valid in the present study, where $V/L\gg 1$. The normalized distribution at all time is $\phi(r,t)\equiv h(r,t)/G(t)$, and for $t\gg 1$ it can be written as

$$\phi(r,t)\simeq\phi_1(t)\begin{cases} \dfrac{1}{t} & \text{for } r\leqslant p(t) \\ 1-\dfrac{\tau}{t}[\ln p(0)-\ln r] & \text{for } p(t)\leqslant r\leqslant p(0) \\ 1 & \text{for } r\geqslant p(0), \end{cases} \tag{B7}$$

where

$$[\phi_1(t)]^{-1}=1+[p(0)-p(t)]/\ln(p(t)/p(0)) =1-\frac{\tau}{t}p(0)[1-\exp(-t/\tau)]. \tag{B8}$$

Equation (B7) is the same as Eq. (31).

[1] U. R. Evans, *The Corrosion and Oxidation of Metals: Scientific Principles and Practical Applications* (Arnold, London, 1960).
[2] H. H. Uhlig, *Corrosion and Corrosion Control* (Wiley, New York, 1963).
[3] D. E. Williams, R. C. Newman, Q. Song, and R. G. Kelly, Nature (London) **350**, 216 (1991).
[4] T. Nagatani, Phys. Rev. A **45**, 2480 (1992).
[5] P. Meakin, T. Jässang, and J. Feder, Phys. Rev. E **48**, 2906 (1993).
[6] R. Reigada, F. Saguès, and J. M. Costa, J. Chem. Phys. **101**, 2329 (1994).
[7] L. Balázs and J-F. Gouyet, Physica A **217**, 319 (1995).
[8] L. Balázs, Phys. Rev. E **54**, 1183 (1996).
[9] B. Sapoval, S. B. Santra, and Ph. Barboux, Europhys. Lett. **41**, 297 (1998); S. B. Santra and B. Sapoval, Physica A **266**, 160 (1999).
[10] D. Stauffer and A. Aharony, *Introduction to Percolation Theory*, 2nd ed. (Taylor & Francis Ltd., London, 1991).
[11] B. Sapoval, M. Rosso, and J. F. Gouyet, J. Phys. (France) Lett. **46**, L149 (1985).
[12] B. Sapoval, M. Rosso, and J. F. Gouyet, in *The Fractal Approach to Heterogeneous Chemistry*, edited by D. Avnir (John Wiley and Sons Ltd., New York, 1989).
[13] H. Saleur and B. Duplantier, Phys. Rev. Lett. **58**, 2325 (1986).
[14] M. Rosso, J. F. Gouyet, and B. Sapoval, Phys. Rev. B **32**, 6053 (1985); R. M. Ziff and B. Sapoval, J. Phys. A **19**, L1193 (1986).
[15] A. Baldassarri, A. Gabrielli, and B. Sapoval (unpublished).
[16] K. J. Falconer, *Fractal Geometry: Mathematical Foundations and Applications* (Wiley, New York, 1990).
[17] T. Grossman and A. Aharony, J. Phys. A **20**, L1193 (1987).
[18] M. Marsili, J. Stat. Phys. **77**, 733 (1994); A. Gabrielli, R. Cafiero, M. Marsili, and L. Pietronero, *ibid.* **84**, 889 (1996).
[19] A. Gabrielli, R. Cafiero, M. Marsili, and L. Pietronero, Europhys. Lett. **38**, 491 (1997).